Applied Catalysis B: Environmental 100 (2010) 472–480

Contents lists available at ScienceDirect

Applied Catalysis B: Environmental

journal homepage: www.elsevier.com/locate/apcatb

Novel CeO_2 promoted TiO_2–ZrO_2 nano-oxide catalysts for oxidative dehydrogenation of p-diethylbenzene utilizing CO_2 as soft oxidant

Komateedi N. Rao[a,b], Benjaram M. Reddy[a], Sang-Eon Park[b,*]

[a] Inorganic and Physical Chemistry Division, Indian Institute of Chemical Technology, Uppal Road, Hyderabad 500 607, India
[b] Laboratory of Nano-Green Catalysis, Inha University, Incheon 402-751, Republic of Korea

ARTICLE INFO

Article history:
Received 17 July 2010
Received in revised form 18 August 2010
Accepted 29 August 2010
Available online 6 September 2010

Keywords:
p-Diethylbenzene
Oxidative dehydrogenation
CO_2 as soft oxidant
TiO_2–ZrO_2 mixed oxide
Acid–base sites

ABSTRACT

The influence of ceria on structural and catalytic properties of TiO_2–ZrO_2 mixed oxide was investigated for oxidative dehydrogenation (ODH) of p-diethylbenzene (DEB) to p-divinylbenzene (DVB) utilizing CO_2 as soft oxidant. The investigated catalysts were synthesized by coprecipitation and impregnation methods involving microwave treatment. Catalyst characterization was achieved using X-ray diffraction (XRD), transmission electron microscopy (TEM), scanning electron microscopy (SEM), BET surface area and temperature programmed desorption/oxidation (TPD/TPO) methods. The XRD and TEM results revealed that the prepared samples are in nanocrystalline form with 10–20 nm size. The presence of acid–base sites and their distribution was examined by NH_3 and CO_2 TPD measurements. The ceria promoted sample exhibited more number of acid sites. The TPO measurements revealed that CO_2 dissociates over the reduced surface of the catalysts. Among various catalysts investigated, the microwave treated CeO_2/TiO_2–ZrO_2 sample exhibited better conversion and a high product selectivity. The time-on-stream studies revealed that ceria promoted TiO_2–ZrO_2 catalysts exhibit higher stability for ODH of DEB.

1. Introduction

One of the most alarming global environmental problems of today is the greenhouse effect. Especially, the global warming instigated by accelerative accumulation of CO_2 in the atmosphere is causing a lot of concern all over the world [1–3]. Therefore, storage and utilization of CO_2 has been identified as a core subject since it provides both environmental and economical benefits. One of the approaches for utilization of CO_2 has been to exploit it as a soft oxidant for catalytic selective oxidation or oxidative dehydrogenation (ODH) of various hydrocarbons to value added products. Due to high endothermic (125 kJ/mol) nature and volume increasing character of ethylbenzene (EB) dehydrogenation (DH) reaction, a large amount of superheated steam is necessary to supply the heat and lower the partial pressure of reactants to shift the equilibrium towards the styrene product. However, much of the latent heat of steam is lost at the gas–liquid separator due to rapid quenching of product as it is necessary. The heat consumption during this high temperature process is a substantial part of the total costs of styrene production. Therefore, there is a great interest to develop better catalysts or a new process that can decrease the reaction temperature and energy consumption significantly.

More recently, several papers emphasized the significance of CO_2 in various reactions as active oxidant, solvent and diluent [4–6]. It is now being established that CO_2 could play several advantageous roles in the ODH reactions. The mechanism of EB ODH reaction with CO_2 has also been fairly established. There are at least two possible pathways for the EB ODH reaction with CO_2 [6]. The reaction can proceed by ODH of EB through oxygen species dissociated from CO_2 in a single step route, and DH of EB coupled with reverse water–gas shift reaction (RWGS) in the two-step process [7–9]. In addition, CO_2 has the highest heat capacity among other typical gases. Therefore, it is very useful for minimizing the hot spot phenomenon on the catalyst surface. It is an established fact that steam leads to loss of a large amount of latent heat upon condensation at a gas–liquid separator following the DH or ODH reactions [10]. Therefore, a soft oxidant like CO_2 is highly desirable for efficient conversion of various hydrocarbons to more useful products in the oxidation reactions.

Recently, a lot of attention has been given to the production of unsaturated hydrocarbons from the reforming feedstocks such as ethylbenzene, diethylbenzene and so on. Especially, the ODH of p-diethylbenzene (DEB) to p-divinylbenzene (DVB) is a significant process owing to several potential applications. In general, the DVB is used as a cross-linking monomer for copolymerization with styrene to produce ion-exchange resins employed in water treatment and in chemical and pharmaceutical industries [11–14]. It is also used in styrene-butadiene rubber to improve the swelling, shrinkage and extrusion properties of the prod-

* Corresponding author. Tel.: +82 32 860 7675; fax: +82 32 872 8670.
E-mail addresses: mreddyb@yahoo.com (B.M. Reddy), separk@inha.ac.kr (S.-E. Park).

0926-3373/$ – see front matter © 2010 Elsevier B.V. All rights reserved.
doi:10.1016/j.apcatb.2010.08.024

uct. At present, the commercial DH of DEB is carried out by using K-doped iron-based catalyst. However, it has to be replaced frequently due to sever deactivation owing to coke formation and leaching of promoters. In addition, a large consumption of energy and lower conversion as well as selectivity are limiting this process. Therefore, there is a lot of interest to find new catalysts or to improve the performance of the existing catalysts. Our recent studies revealed that TiO_2–ZrO_2 mixed oxides are very active and stable for ODH and dehydrocyclization reactions [6,15–19]. As reported in the literature the combined TiO_2–ZrO_2 mixed oxides exhibit acid–base properties together, hence, were exploited for various catalytic applications [18]. It is well-known from the literature that ceria is one of the best used promoter to improve the oxidation ability as well as acid–base properties of several catalytic systems [20–25]. The unique oxygen storage/release capacity (OSC) and redox properties of ceria are known to suppress the deactivation of catalysts under rigorous reaction conditions.

The present investigation was undertaken against the aforementioned background. In this study TiO_2–ZrO_2 and CeO_2 promoted TiO_2–ZrO_2 catalysts were synthesized by both microwave and hydrothermal methods and evaluated for the ODH of DEB using CO_2 as mild oxidant. To understand the advantage of microwave dielectric heating over conventional heating, both methods were adopted for making of samples. To examine the physicochemical properties of the samples synthesized, various characterization techniques namely, BET surface area (SA), X-ray diffraction (XRD), temperature programmed desorption (TPD) of CO_2 and NH_3, temperature programming reduction (TPR) followed by oxidation with CO_2 (H_2 TPR–CO_2 TPO), transmission electron microscopy (TEM), scanning electron microscopy (SEM) and X-ray photoelectron spectroscopy (XPS) were employed. To understand the deactivation phenomenon of catalysts, the spent catalysts were also subjected to XRD, SEM and thermogravimetric (TG) analysis.

2. Experimental

2.1. Catalyst preparation

Unpromoted TiO_2–ZrO_2 (1:1 mole ratio) and 2 wt.% ceria promoted TiO_2–ZrO_2 mixed oxide samples were synthesized by a conventional co-precipitation method. In a typical experiment, the requisite quantities of zirconyl(IV) nitrate hydrate (Acros Organics, USA), titanium(IV) chloride (Yakuri Pure Chemicals, Japan) and ammonium ceric(IV) nitrate (TCI, Japan) were dissolved separately in deionized water and mixed together. Cold titanium(IV) chloride was digested first in cold concentrated HCl and diluted with deionized water. To the mixture solution, sodium hydroxide (3 M) was added drop wise until the precipitation was complete and the resultant precipitate was stirred vigorously for 24 h. Thus obtained slurry was divided into two equal parts and one portion was transferred to round bottom flask and aged hydrothermally for 24 h at 100 °C with continuous stirring [5,6,26]. Remaining portion was subjected to microwave energy (300 W) at 100 °C for 1 h. The obtained precipitates were finally filtered off and washed several times with deionized water until free from anion impurities. The resulting materials were oven dried at 120 °C for 12 h and subsequently calcined at 550 °C for 5 h in air atmosphere. Some portions of the finished samples were again heated at 750 °C for 5 h to investigate their thermal stability. The labeling of the synthesized materials is as follows: microwave treated TiO_2–ZrO_2 (TZ MW), hydrothermal treated TiO_2–ZrO_2 (TZ HT), microwave treated 2 wt.% CeO_2/TiO_2–ZrO_2 (CTZ MW) and hydrothermal treated 2 wt.% CeO_2/TiO_2–ZrO_2 (CTZ HT).

2.2. Catalyst characterization

Powder X-ray diffraction patterns were recorded on a Rigaku Multiflex instrument using nickel-filtered Cu Kα (0.15418 nm) radiation source and a scintillation counter detector. The intensity data were collected over a 2θ range of 2–80° with a 0.02° step size and using a counting time of 1 s per point. Crystalline phases were identified by comparison with the reference data from International Center for Diffraction Data (ICDD) files. The BET surface area measurements were made by N_2 adsorption/desorption at liquid-nitrogen temperature using a Micromeritics ASAP 2020 instrument. Before analysis, samples were evacuated for 3–4 h at 250 °C in the degassing port of the instrument. TG analysis of used samples was carried using SDT Q600 V20.9 Build 20 instrument from ambient temperature to 1000 °C. The XPS measurements were made on a KRATOS (ESCA AXIS 165) spectrometer by using Mg Kα (1253.6 eV) radiation as the excitation source. The SEM images were collected with a JEOL 630-F microscope. Before measurements, samples were dispersed on a steel plate surface and coated with Pt metal. The TEM images were obtained on a JEM-2010 (JEOL) instrument equipped with a slow-scan CCD camera and at an accelerating voltage of 400 kV. Samples were sonically dispersed in ethanol and deposited on a carbon coated copper grid before examination.

The TPD and H_2 TPR followed by CO_2 TPO measurements were made on a Pulse Chemisorb 2705 (Micromeritics, USA) instrument. Before the measurements, samples were preconditioned at 300 °C for 2 h. For TPD measurements, 5% CO_2 in He or 5% ammonia in He was adsorbed at 50 °C for 60 min and purged at the same temperature with helium gas (20 ml/min) to remove the physisorbed gas. The TPD run was then conducted from 50 to 800 °C at a heating rate of 10 °C/min. To understand CO_2 dissociation over the catalysts, H_2 TPR followed by CO_2 TPO was performed. For this purpose, the H_2-TPR measurement was carried out using 5% H_2 in Ar, subsequently the sample was cooled in He atmosphere and again heated in 5% CO_2 in He (30 ml/min) from 50 to 800 °C.

2.3. Catalyst activity

The catalytic activity for vapour phase ODH of DEB was investigated in a down flow fixed-bed stainless steel microreactor. For each run, 0.5 g of sample was loaded in the reactor with 0.5 g of glass beads. The reactor was heated to 600 °C at a rate of 10 °C/min in the flow of He (20 ml/min) and kept at this temperature for 2 h and He was replaced with CO_2 gas. The catalyst pretreatment was continued at 600 °C for 1 h with CO_2 (20 ml/min) before conducting the reaction. The DEB was introduced into the preheating zone of the reactor through a liquid feed pump with a constant feed rate of 0.5 ml/h. Gaseous and liquid products were analyzed simultaneously by an on-line gas chromatograph (Younlin Instrument, Acme 6000 Series, Korea) equipped with TCD and FID. For analysis of liquid products, HP-innowax column (30 m long, 0.32 mm i.d. and 0.25 μm film thickness) was employed and for gaseous products Porapak N 80/100 column (6 ft × 1/8 in.) was used. The main gaseous products detected were hydrogen, ethylene, methane, carbon monoxide and carbon dioxide.

3. Results and discussion

3.1. XRD and XPS

The XRD patterns of TiO_2–ZrO_2 (TZ) and CeO_2/TiO_2–ZrO_2 (CTZ) samples calcined at 550 and 750 °C are shown in Figs. 1 and 2, respectively. As can be seen from the figures, there are no obvious peaks corresponding to individual oxides such as CeO_2, ZrO_2 and TiO_2. The absence of ZrO_2 and TiO_2 peaks in the mixed oxides

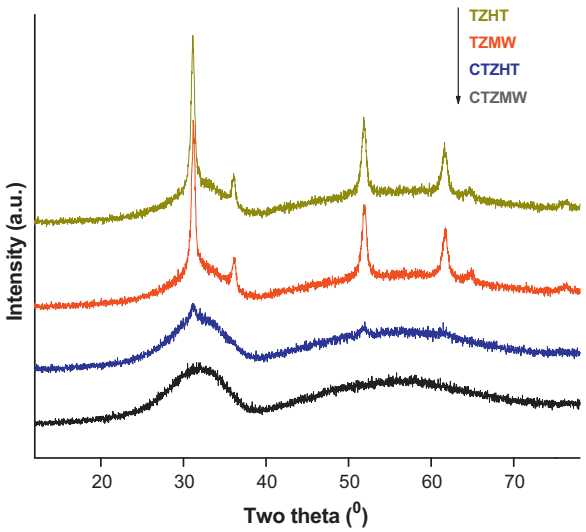

Fig. 1. X-ray powder diffraction patterns of various catalysts calcined at 550 °C. TiO_2–ZrO_2 (TZ); 2 wt.% CeO_2/TiO_2–ZrO_2 (CTZ); microwave (MW); hydrothermal (HT) treatment.

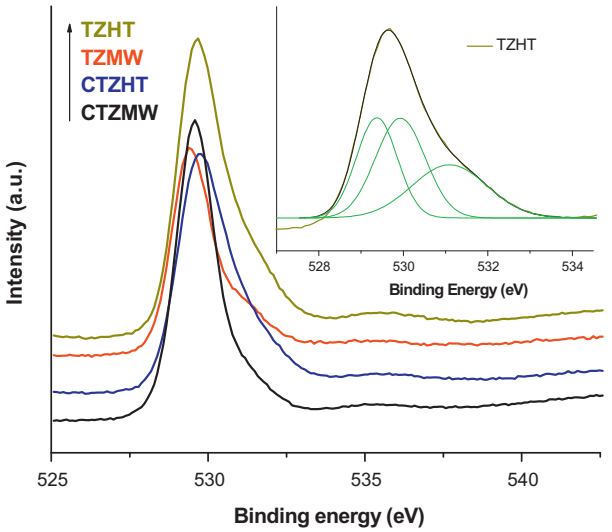

Fig. 3. O 1 s core level XPS profiles of TiO_2–ZrO_2 (TZ) and 2 wt.% CeO_2/TiO_2–ZrO_2 (CTZ) calcined at 550 °C.

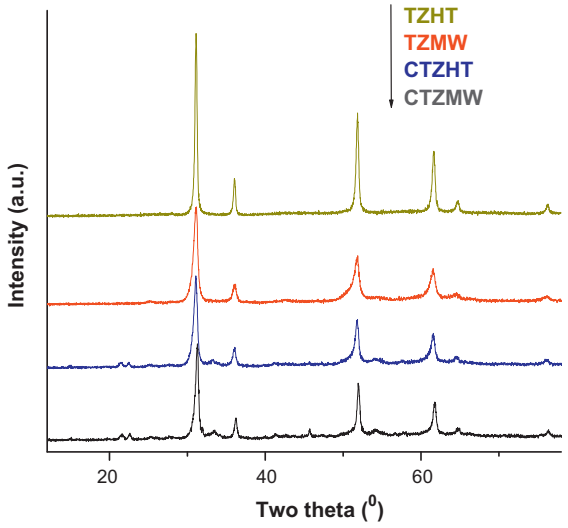

Fig. 2. X-ray powder diffraction patterns of various catalysts calcined at 750 °C. TiO_2–ZrO_2 (TZ); 2 wt.% CeO_2/TiO_2–ZrO_2 (CTZ); microwave (MW); hydrothermal (HT) treatment.

implies that these oxides are distributed homogeneously and the broad peaks reveal poor crystallinity of the TiO_2–ZrO_2 hybrid catalyst. The observed peaks at $2\theta = 30.8°$, 36.0°, 51.3°, 61.2°, 64.9° and 76.0° (JCPDS 08-0352) are due to $TiZrO_4$ phase [5,6,18]. Both series of TZ and CTZ samples showed predominant XRD peaks corresponding to the $TiZrO_4$ phase even after treating the samples at 750 °C. In general, at this temperature pure TiO_2 undergoes a phase transformation from anatase to rutile, usually begins at 500 °C [27,28]. There is no such transformation from these results which suggest that the addition of ZrO_2 and TiO_2 together is effective in enhancing the thermal stability of both the oxides. The ceria-based catalysts (CTZ) showed broader peaks, which can be assigned to the amorphous nature of the formed solids. In particular, to understand the thermal behavior of the materials, samples were treated at 750 °C. The 750 °C calcined samples exhibited an increase in the intensity of the peaks due to better crystallization. However, the crystalline phases in all the samples could be assigned to the $TiZrO_4$ phase only. Tajima et al. [29] investigated the XRD patterns of various TiO_2–ZrO_2 binary oxides having different compositions. An amorphous phase was observed for TZ-55/45 composition and a crystalline $ZrTiO_4$ for TZ-58/42. The TZ-70/30, TZ-82/18 and TZ-90/10 compositions were mixtures of $ZrTiO_4$ and the anatase-type TiO_2 crystals. The present results are in line with earlier findings. The peak intensity of the lines due to $ZrTiO_4$ increased with increasing calcination temperature indicating crystal growth of $ZrTiO_4$. The average crystallite diameter of Zr–Ti oxides were estimated from the width of the peaks by using Scherrer equation (see Table 1). Increasing the calcination temperature of the samples, lead to a moderate increase in the crystallite size. However, in all cases the crystallite size remained smaller than 20 nm.

To investigate the surface composition of various catalysts, XPS measurements were performed and the corresponding binding energy values pertaining to Zr 3d and Ti 2p are listed in Table 1. As shown in Table 1, the core level electron binding energy of Ti 2p observed at around 458 eV correspond to the spin orbital multiplet of Ti $2p_{3/2}$ [6,15]. The XPS peak corresponding to Zr $3d_{5/2}$ is observed at around 181.5 eV. Both Zr 3d and Ti 2p binding energies reveal the presence of 4+ oxidation state for Zr and Ti in the samples. The O 1s core level XPS profiles of various samples after thermal treatment at 550 °C are shown in Fig. 3. As can be

Table 1
BET surface area, XPS binding energy and crystallite size values of various samples prepared by microwave (MW) and hydrothermal (HT) treatments: TiO_2–ZrO_2 (TZ); 2 wt.% CeO_2/TiO_2–ZrO_2 (CTZ).

Catalyst	BET SA ($m^2\ g^{-1}$)	Binding energy (eV)		Crystallite size (nm)		
		Zr $d_{5/2}$	Ti $2p_{3/2}$	550 °C	750 °C	Used
TZ HT	48	181.7	458.1	14.4	18.1	14.6
TZ MW	31	181.5	457.9	14.1	14.7	17.5
CTZ HT	56	181.7	458.1	–	14.9	–
CTZ MW	70	181.6	458.1	–	17.7	–

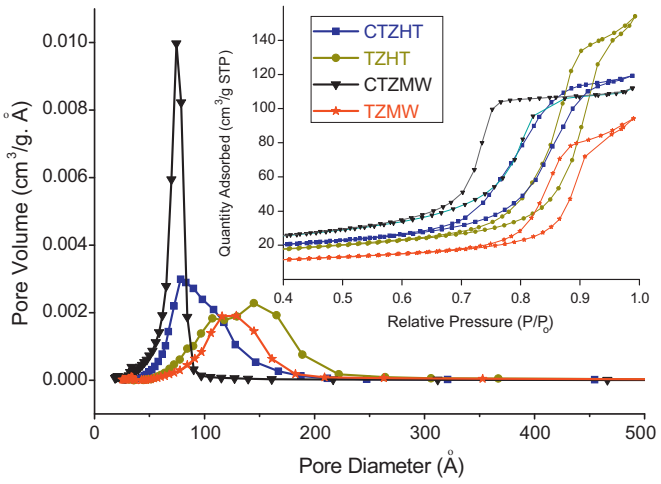

Fig. 4. N_2 sorption isotherms (inset) and corresponding BJH pore-size distribution curves of various samples calcined at 550 °C.

observed from this figure, all profiles are characterized by broad peaks in the range of 527–533 eV. In general, the O 1s profile is more complicated due to the overlapping contribution of oxygen from titania, zirconia and $TiZrO_4$. The fwhm of O 1s spectra are approximately equal to 1.8 eV, hence the bands were fitted into three main signals. For better understanding, a deconvolution profile of TZ HT is shown in the inset. The first signal at about 529 eV is attributed to O in TiO_2, second peak at 530.3 eV corresponds to ZrO_2 and the peak at 532 eV could be assigned to the oxygen binding energy from hydroxyl groups [18,30]. The unsymmetrical nature and larger fwhm of the O 1s peak indicates the existence of high concentration of hydroxyl groups, which further emphasize the presence of more defects over the surface [30–32]. The higher binding energy peak (532 eV) contains components resulting from the hydroxylation of the metal oxides. There is a possibility of acidic and basic hydroxyl groups at the outermost surface as well as adsorbed water. The hydroxyl oxygen is most important for the title reaction. Hence, the probable formation of OH groups was considered in the estimation of oxygen binding energy. However, it has been noted that the binding energy of third signal is also close to the terminal oxygen of Brønsted acidic sites (M–OH). It is well-known that the XPS peak intensity depends on both ion density and its chemical environment. The oxygen ion density in various samples is expected to be same. Therefore, the decrease in the peak intensity can be attributed to different chemical environments [19,22].

3.2. BET surface area and TEM analysis

In order to understand the pore structure of the catalysts, the N_2 adsorption–desorption measurements were carried out. The corresponding pore size distribution isotherms of 550 °C calcined samples are shown in Fig. 4. The obtained isotherms (inset) are almost similar for all samples which could be identified as type IV. The increase in adsorbed volume at high relative pressure is a direct indication of the presence of the secondary large pores [16,28]. In general, all synthesized samples exhibited broad pore size distribution peaks. However, the CTZ MW sample showed sharp and small pore diameter indicating the presence of mesoporosity with larger pore volume thereby high specific surface area. The mesopore size has significant role on the adsorption properties of reactant molecules and thereby it can play a major role in the activity. The BET specific surface areas of 550 °C calcined samples are shown in Table 1. The specific surface areas of TZ samples are found to be in the range of 48–69 $m^2\ g^{-1}$. Addition of nominal amount of ceria to TZ improved the surface area as well as the textural properties of the sample.

The representative TEM images of various samples calcined at 550 °C are shown in Fig. 5. The TZ sample revealed a homogeneous distribution of crystallites all over the surface. The statistical determination done by counting the crystallites indicated a mean particle size of 15.2 nm, which is close to the numeral values obtained by XRD technique (~14 nm). This observation reveals that the particles are uniformly distributed over the whole solid. The ceria promoted samples also exhibited nanocrystalline particles. However, as compared to the pure TZ, the particle size of ceria promoted samples is smaller. The TEM micrographs further showed that these oxides are in more densely packed configuration and prone to crystallization, as the particles exhibit some sharp edges that are indicative of sintering to bigger crystallite formation. Regarding the morphology, these oxides seem to be configured by a stack of spherical particles. In case of TZ sample, the particle sizes ranged between 20 and 30 nm and in more number compared to the particles of 6–10 nm size in the case of CTZ sample. Many randomly oriented nano-crystallites with sets of clearly resolved lattice fingers are observed. These results indicate that introduction of CeO_2 can effectively inhibit the excessive crystal growth and stabilizes the porous structure. The TEM results are in line with XRD and N_2-sorption measurements.

3.3. TPD of CO_2 and NH_3

The acid–base properties of the oxide catalysts are very important for the development of scientific criteria in catalytic applications. In an attempt to connect the effect of structure of the nano-composite oxides on the acid–base properties, the acidity and basicity of the samples were measured by NH_3- and CO_2-TPD experiments, respectively. Fig. 6 represents the ammonia-TPD profiles of microwave and hydrothermally treated TZ and CTZ samples. In general, the maximum NH_3 desorption peaks for ZrO_2 and TiO_2 samples are observed at around 182 and 310 °C, respectively [33,34]. The sites of weak, medium and strong acid strength are characterized by desorption of ammonia at <200 °C, 200–300 °C and >350 °C, respectively [34]. The ammonia desorption peak maxima of CTZ sample is located at around 180 °C, which is slightly higher when compared to that of TZ sample. However, with the addition of ceria to TZ a large desorption signal is observed for both microwave and hydrothermal treated samples indicating that ceria enhanced the acid sites of the pure support. The formation of more number of acid sites is probably due to the substitution of some titanium and zirconium by cerium atoms or due to the influence of better dispersion of CeO_2 over the TZ support. Concerning the strength of acid sites, it is accepted that desorption temperature could be related to the strength of the sites. In the case of mixed oxides, the maximum desorption temperature for TZ were observed at 126 and 380 °C, while for ceria promoted samples the same were observed at around 200 and 430 °C, respectively. With a small exception, the strength of the acid sites of microwave and hydrothermal treated samples are in the same order. Further, from these results one can speculate the presence of Brønsted acid sites, since it has been reported that the desorption temperatures higher than 400 °C correspond to Brønsted acid sites [33,35]. The TPD and XPS results are found to corroborate well with each other. It is known that as transition metal oxide particle size decreases the number of surface oxygen anion vacancies increases, hence new and stronger acid sites are created, with particles of smallest diameter having the strongest acidity [36]. Therefore, the present mixed oxides, which are a mixture of relatively smaller particles, are expected to contribute to the acidity from anion vacancies. The basic strength distribution of catalysts was analyzed by CO_2-TPD technique. Fig. 7 displays the CO_2-TPD profiles of various samples calcined at 550 °C. Ceria

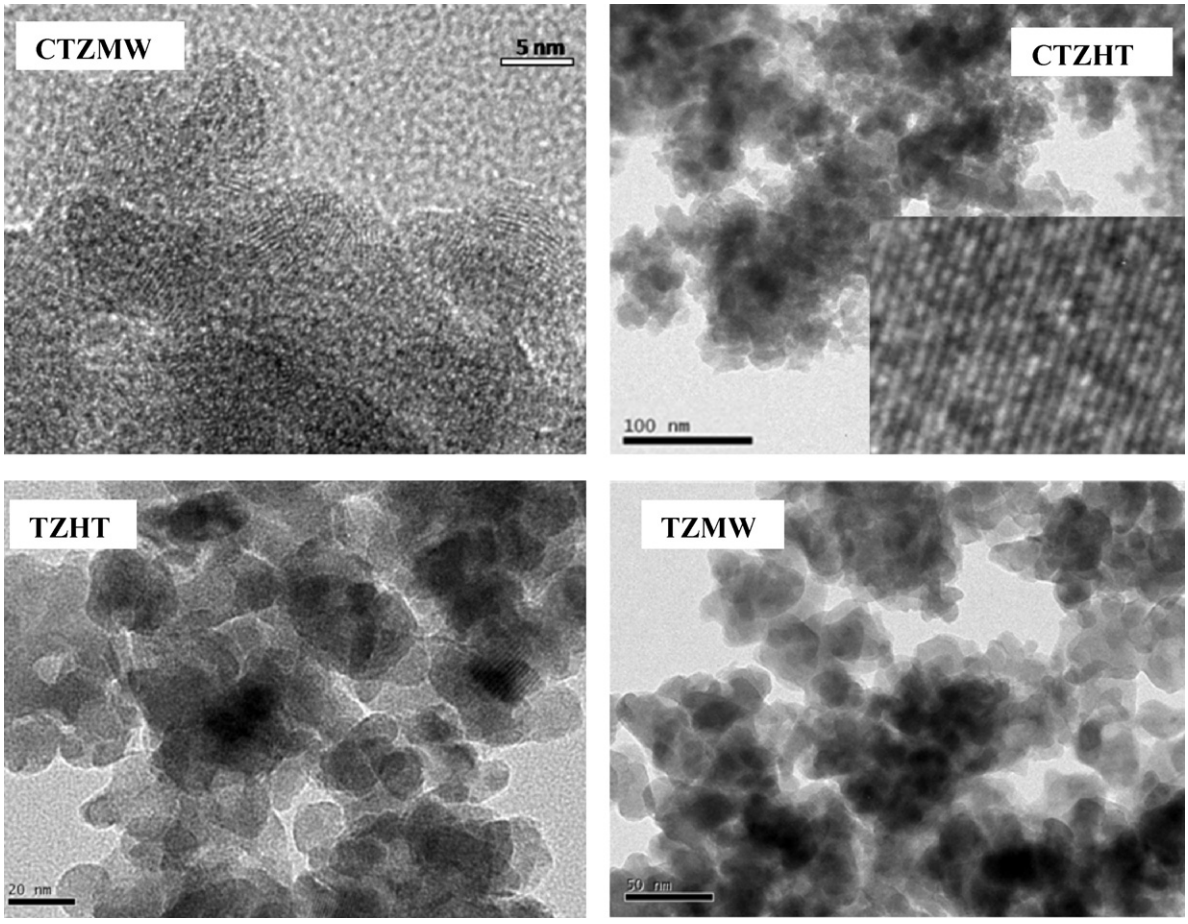

Fig. 5. TEM images of TiO_2–ZrO_2 (TZ) and 2 wt.% CeO_2/TiO_2–ZrO_2 (CTZ) samples calcined at 550 °C.

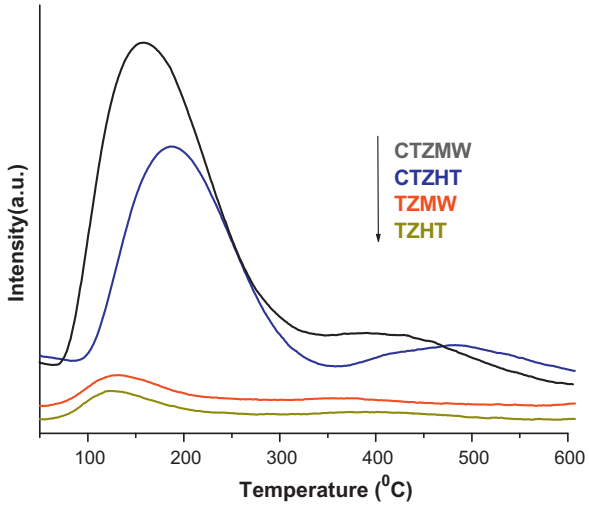

Fig. 6. NH_3 TPD profiles of TiO_2–ZrO_2 (TZ) and 2 wt.% CeO_2/TiO_2–ZrO_2 (CTZ) samples calcined at 550 °C.

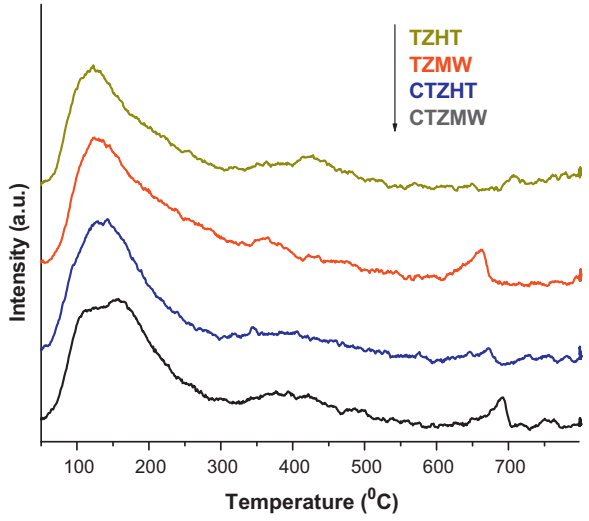

Fig. 7. CO_2 TPD profiles of TiO_2–ZrO_2 (TZ) and 2 wt.% CeO_2/TiO_2–ZrO_2 (CTZ) samples calcined at 550 °C.

promoted and unprompted TiO_2–ZrO_2 samples showed two prominent signals; one at 90–250 °C (highest) and another at around 400 °C (small) [16,33,34]. The distribution of acidic and basic sites is fairly similar in all the samples, even though the strength of acidity is more compared to the basicity of ceria promoted samples. It is apparent from these results that the addition of CeO_2 improves the acid–base properties of TZ mixed oxides.

3.4. H_2 TPR–CO_2 TPO results

According to thermodynamics, the gas phase dissociation of CO_2 to CO and O_2 is very difficult [37,38]. CO_2 promotes oxidation via the formation of monoatomic oxygen species adsorbed on the catalyst surface. This species would form by dissociative adsorption of CO_2 on the catalyst surface ($CO_2 \rightarrow CO + O$). It is proposed that CO_2 adsorption and subsequent dissociation on transition metals pro-

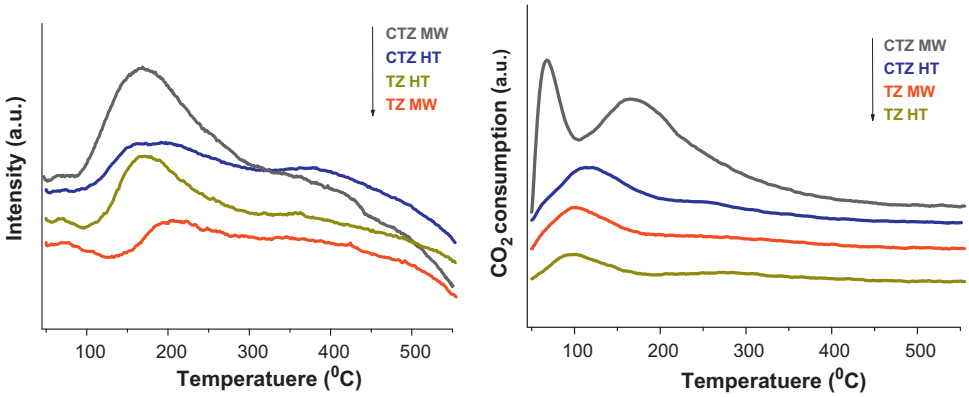

Fig. 8. H_2 TPR-CO_2 TPO profiles of TiO_2–ZrO_2 (TZ) and 2 wt.% CeO_2/TiO_2–ZrO_2 (CTZ) samples calcined at 550 °C.

ceed through electron transfer from metal to CO_2 molecule to form an anion radical species, $CO_2^{\bullet-}$ [39,40]. The charge polarization in CO_2 makes the carbon atom acidic, by which the addition of oxygen to carbon atom of CO_2 facilitates both adsorption in the form of carbonates and dissociation [37]. It is also reported that the activation of CO_2 molecules is structure sensitive [41,42]. A crucial experiment to prove the oxidizing role of CO_2 was performed by CO_2 TPO using a reduced catalyst. Fig. 8 displays the H_2-TPR (left) and CO_2-TPO (right) profiles of various samples investigated. As shown in Fig. 8 (left), a broad peak due to the reduction of surface oxides has been observed. There is a negative peak at around 550 °C that could be attributed to release of substrate by the support or from the formation of new phase as TPR temperature is higher than the original calcination temperature [5,6]. After the reduction, samples were re-oxidized with CO_2 and the obtained plots disclosed a low temperature and a high temperature oxidation signal. In addition, these peaks are high intense for CTZ MW sample, and low intense and towards higher temperature side for other samples. This could be due to high specific surface area and more number of acid–base sites available on the CTZ MW sample surface. Two types of CO_2 consumption signals also indicate the presence of different oxidizable species over these materials. In agreement with the present results, Pokrovski et al. [43] also noticed a high CO_2 adsorption capacity due to strong Lewis acidity and basicity as well as high specific surface area. From these results it can be concluded that the prepared materials dissociate the CO_2 to some extent. Further studies are necessary to clarify the exact role of ceria and the CO_2 dissociation mechanism over the practical catalysts.

3.5. Activity results

The ODH of DEB was carried out in the vapor phase at normal atmospheric pressure using CO_2 as soft oxidant. Over all catalysts with increase of reaction temperature an increase in the DEB conversion was observed, since it is an endothermic reaction. The conversion and selectivity results of various catalysts are shown in Table 2. As could be noted from the table, the catalytic results are highly promising in terms of total selectivity of dehydrogenated products in all cases. For better understanding, the reaction data after 3 h of reaction were compared. Usually, the DEB dehydrogenation proceeds in two steps; the first step of DEB dehydrogenation to ethyl vinyl benzene (EVB) is much easier than the second step of ethyl styrene (EST) dehydrogenation to DVB. As known from the literature, in the absence of CO_2 as oxidant the DH or ODH reactions lead to nonselective products and facilitate faster deactivation of the catalyst. If CO_2 is introduced the deactivation of catalysts drops down drastically and selectivity of the products increases over prolonged times. Therefore, these observations could be used as a good basis to explain the better performance of the present catalysts [39]. However, with an increase in reaction temperature (above 600 °C) the selectivity of DVB and EVB were considerably decreased due to thermal cracking of DEB and other products [11,44]. As known, at higher temperatures there is a possibility of formation of higher amounts of toluene, benzene and other polyaromatics which deposit on the surface/pores of the samples that lead to severe fall in the DVB selectivity. Among all catalysts examined, the

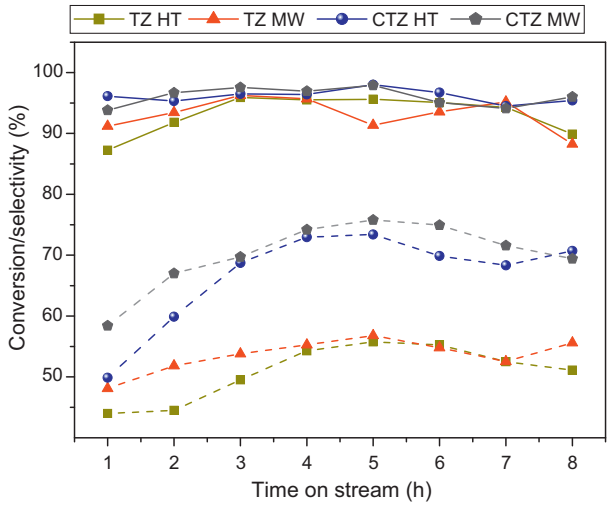

Fig. 9. Variation of catalytic activity and selectivity with time-on-stream. TiO_2–ZrO_2 (TZ); 2 wt.% CeO_2/TiO_2–ZrO_2 (CTZ); microwave (MW); hydrothermal (HT) treatment. Reaction conditions: T = 600 °C, P = 1 atm, LHSV = 0.5 ml/h, CO_2/DEB = 20 (molar ratio).

Table 2
Conversion of DEB, selectivity of EVB, DVB and EVB + DVB, and coke deposition results of various catalysts. Reaction conditions: T = 600 °C, P = 1 atm, LHSV = 0.5 ml/h, CO_2/DEB = 20 (molar ratio).

Catalyst	Conversion of DEB (%)	Selectivity of EVB (%)	Selectivity of DVB (%)	Total selectivity (%)	Coke (%)
TZ HT	54	68	28	96	9.0
CTZ HT	73	65	32	97	7.6
TZ MW	55	67	28	95	12.8
CTZ MW	74	66	33	99	12.5

CTZ MW sample showed better catalytic activity in terms of conversion and product selectivity. The observed better activity could be attributed to high specific surface area, better redox nature and profound acid–base properties of the catalyst.

To understand the catalyst stability and product distribution, for instance, time-on-stream experiments were performed. Generally, a faster catalyst deactivation is often encountered on most of the catalytic systems in the DH or ODH reactions due to coke formation. Thus, time-on-stream studies are very useful to understand the behavior of the catalysts. Fig. 9 shows the variation of DEB conversion and selectivity on various catalysts at different time intervals. The dotted lines indicate the conversion of reactant and thick lines represent the selectivity of total dehydrogenated products. As could be seen from the figure, the conversion of DEB increased in the first few hours. Initially, the increase in the conversion is due to formation of thin layer of carbonaceous species over the surface, which promotes the DH reaction [39,44]. Additionally, the selectivity of total DH products is maintained at around 95% without any decrease during the time-on-stream experiments. The observed stable selectivity revealed that the active sites over the surface of these catalysts are unaffected by coke formation or other side products formation. The CTZ MW sample showed excellent conversion as well as product selectivity. The time-on-stream results indicated that the synthesized catalysts are highly stable and active for the ODH of DEB. To gain information regarding the deactivation phenomenon of these catalysts, the spent catalysts (after time-on-stream experiments) were subjected to TG, XRD and SEM analysis and the corresponding discussion is presented below.

3.6. Deactivation studies

The XRD patterns of spent catalysts are depicted in Fig. 10. As could be noted from the figure, the TZ samples exhibited XRD peaks

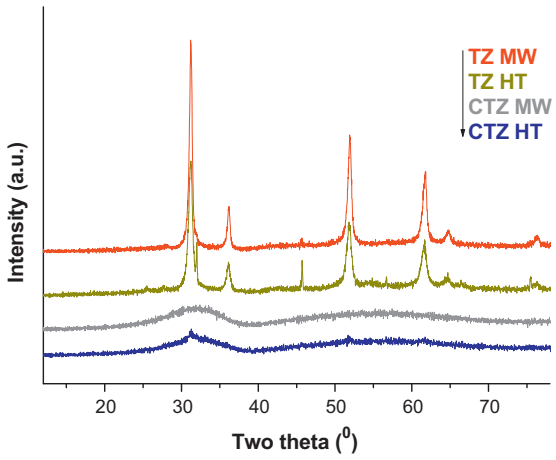

Fig. 10. X-ray powder diffraction patterns of used TiO_2–ZrO_2 (TZ) and 2 wt.% CeO_2/TiO_2–ZrO_2 (CTZ) samples after 8 h of time-on-stream measurements.

mainly corresponding to $TiZrO_4$ phase. There are no extra specific lines in the spent CTZ samples and they look like the fresh samples calcined at 550 °C. The existence of used catalysts in amorphous or poorly crystalline form signifies the promotional effect of ceria on the stability of the catalysts. In addition, the crystallite sizes of these samples are also analogous to 550 °C calcined samples (Table 1). The coke deposition over the samples was investigated by means of TG analysis, and the resulting values pertaining to various samples are presented in Table 2. The amount of coke deposited is observed to be unsymmetrical and no specific correlation is apparent. The TG analysis showed a weight loss signal at around 270–450 °C attributed to non-crystalline coke deposition mainly due to cracking of products, further, up to 700 °C there is no considerable loss in the mass [39]. To know the morphol-

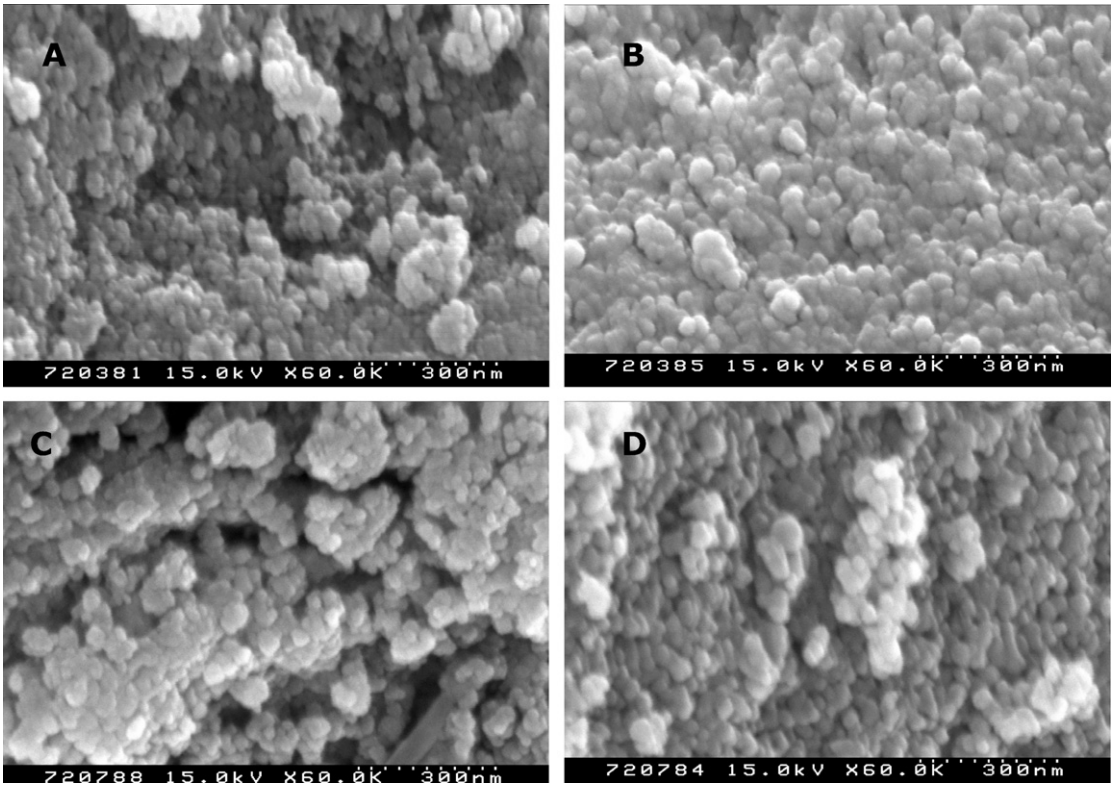

Fig. 11. SEM images of fresh TiO_2–ZrO_2 (TZ) HT (A) and CeO_2/TiO_2–ZrO_2 (CTZ) HT (B); and used TiO_2–ZrO_2 (TZ) HT (C) and CeO_2/TiO_2–ZrO_2 (CTZ) HT (D) catalysts after 8 h of time-on-stream measurements.

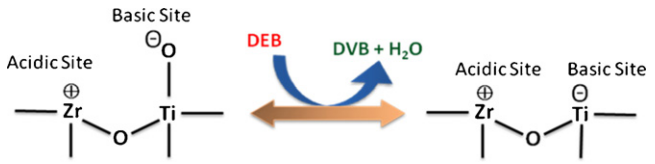

Scheme 1.

ogy of the used catalysts, SEM analysis was performed and the representative SEM images of various samples are displayed in Fig. 11. This figure reveals spherical aggregates of smaller particles with uniform particle size. It can also be observed that the particles are with rough surface. Except few carbonaceous species over the surface, the morphology of the used catalysts did not differ significantly from the fresh samples. In conclusion, it is clear from these results that the addition of nominal percentage of ceria over the titania-zirconia influenced the structural, electronic and catalytic properties of the parent oxides. The deactivation studies revealed that the thermal stability and mechanical strength of the synthesized samples did not change during the time-on-stream runs.

In the present investigation, we made an attempt to correlate the CO_2 dissociation with the ODH activity. The dissociation of CO_2 under our experimental conditions is very low. In spite of that the influence of such dissociation appears to be very important. Based on the reports found in the literature, and from the TPD and H_2 TPR–CO_2 TPO results, a possible bifunctional mechanism is proposed [17,34,45]. Accordingly, Scheme 1 represents the adjacent electron-acceptor and electron-donor sites over the TZ sample. These acidic and basic sites are expected to play a promising role in the ODH reaction. In this scheme, the structure A (left) is transformed into structure B (right) by converting DEB to EVB. Further, the DH of EVB provides the DVB. Structure B is converted back to structure A by taking the lattice oxygen that could be formed from dissociation of CO_2. The acid–base and redox properties of the catalysts are expected to play a major role in this reaction.

4. Conclusions

In the present investigation, unpromoted TiO_2–ZrO_2 and ceria promoted TiO_2–ZrO_2 mixed oxides were synthesized by a co-precipitation method involving thermal or microwave energy and subjected to calcination at 550 and 750 °C. The resulting samples were characterized by various physicochemical techniques. The resultant catalysts exhibited moderate specific surface area, in particular, CTZ MW sample showed high specific surface area and large pore volume. The standard XRD patterns revealed the formation of $TiZrO_4$ when the samples were calcined at 750 °C. With increase in calcination temperature a slight increase in the crystallite size has been observed. The XPS profiles of Ti 2p and Zr 3d revealed the presence of Ti^{4+} and Zr^{4+} oxidation states. The unsymmetrical nature and large fwhm of O 1s peak indicated the presence of high concentration of hydroxyl groups, which further emphasize more structural defects in the samples. The nanosized (10–20 nm) particles with randomly oriented nano-crystallites were manifested from TEM images. The XRD and TEM measurements clearly showed that the addition of 2 wt.% ceria to titania-zirconia influences the specific surface area and particles size of the TZ samples. Ammonia TPD data suggested a profound improvement in the acidic sites of TZ sample up on the addition of ceria. There were no characteristic XRD lines corresponding to CeO_2 indicating that ceria is in a highly dispersed form. The CO_2-TPO results evidenced that the CO_2 dissociates over the reduced surface of the catalysts. Among various catalysts investigated, the CTZ MW sample showed a high conversion (74%) and excellent product selectivity (98%). The time-on-stream results confirmed the stability of these materials up to 8 h of continuous reaction. The CeO_2 promoted TiO_2–ZrO_2 mixed oxides are highly promising for the title reaction owing to the salient features of high specific surface area, profound surface acid–base properties, a high thermal stability and strong mechanical strength. Further studies are under active progress to exploit these catalysts for commercial scale utilization.

Acknowledgements

KNR thanks Inha Industry Partnership Institute for inviting him as a guest PhD student. This work was supported by National Research Foundation of Korea (NRF) funded by the Korea government (MEST) (2009-0083073) and Ministry of Knowledge Economy (MKE).

References

[1] D.-Y. Hong, S.H. Jhung, J.-M. Lee, M.-S. Park, J.-S. Chang, S.-E. Park, Stud. Surf. Sci. Catal. 153 (2004) 333–338.
[2] C.T. Yavuz, B.D. Shinall, A.V. Iretskii, M.G. White, T. Golden, M. Atilhan, P.C. Ford, G.D. Stucky, Chem. Mater. 21 (2009) 3473–3475.
[3] E.H. Lee, Catal. Rev. Sci. Eng. 8 (1973) 285–305.
[4] C.-S. Hwang, N.-C. Wang, Mater. Chem. Phys. 88 (2004) 258–263.
[5] J.-C. Wu, C.-S. Chung, C.-L. Ay, I. Wang, J. Catal. 87 (1984) 98–107.
[6] K.N. Rao, B.M. Reddy, B. Abhishek, Y.-H. Seo, N. Jiang, S.-E. Park, Appl. Catal. B: Environ. 91 (2009) 649–656.
[7] S. Chen, A. Sun, Z. Qin, J. Wang, Catal. Commun. 4 (2003) 441–447.
[8] Z. Qin, J. Liu, A. Sun, J. Wang, Ind. Eng. Chem. Res. 42 (2003) 1329–1333.
[9] M.E.E. Abashar, Chem. Eng. Proc. 43 (2004) 1195–1202.
[10] A. Sun, Z. Qin, S. Chen, J. Wang, J. Mol. Catal. A: Chem. 210 (2004) 189–195.
[11] J.S. Yoo, Appl. Catal. A: Gen. 142 (1996) 19–29.
[12] F.M. Bautista, J.M. Campelo, D. Luna, J.M. Marinas, R.A. Quirós, A.A. Romero, Appl. Catal. B: Environ. 70 (2007) 611–620.
[13] A. Fihri, R. Durand, F. Renzo, F. Fajula, B. Coq, T.-M. Roussel, B. Vuillemin, Appl. Catal. B: Environ. 98 (2010) 224–228.
[14] A.S. Say, G.M. Phanse, US Patent 6,388,155 (2002).
[15] B.M. Reddy, B. Chowdhury, I. Ganesh, E.P. Reddy, T.C. Rojas, A. Fernandez, J. Phys. Chem. B 102 (1998) 10176–10182.
[16] H. Imagawa, T. Tanaka, N. Takahashi, S. Matsunaga, A. Suda, H. Shinjoh, J. Catal. 251 (2007) 315–320.
[17] I. Wang, W.-F. Chang, R.-J. Shiau, J.-C. Wu, C.-S. Chung, J. Catal. 83 (1983) 428–436.
[18] B.M. Reddy, A. Khan, Catal. Rev. Sci. Eng. 47 (2005) 257–296.
[19] H. Imagawa, N. Takahashi, T. Tanaka, S. Matsunaga, H. Shinjoh, Appl. Catal. B: Environ. 92 (2009) 23–29.
[20] D. Haffad, A. Chambellan, J.C. Lavalley, J. Mol. Catal. A: Chem. 168 (2001) 153–164.
[21] O. Demoulin, M. Navez, J.-L. Mugabo, P. Ruiz, Appl. Catal. B: Environ. 70 (2007) 284–293.
[22] B.M. Reddy, K.N. Rao, G.K. Reddy, A. Khan, S.-E. Park, J. Phys. Chem. C 111 (2007) 18751–18758.
[23] B. Hu, Z. Zeng, X. Yang, L. Mao, Y. Euang, Nucl. Instrum. Meth. Phys. Res. Sec. B: Beam Interact. Mater. Atoms 76 (1993) 178–179.
[24] B.M. Reddy, P. Bharali, P. Saikia, A. Khan, S. Loridant, M. Muhler, W. Grunert, J. Phys. Chem. C 111 (2007) 1878–1881.
[25] B. Murugan, A.V. Ramaswamy, J. Am. Chem. Soc. 129 (2007) 3062–3063.
[26] T.P. Braga, E. Longhinotti, A.N. Pinheiro, A. Valentini, Appl. Catal. A: Gen. 362 (2009) 139–146.
[27] H. Zou, Y.S. Lin, Appl. Catal. A: Gen. 265 (2004) 35–42.
[28] P. Afanasiev, Catal. Commun. 9 (2008) 734–739.
[29] M. Tajima, M. Niwa, Y. Fujii, Y. Koinuma, R. Aizawac, S. Kushiyama, S. Kobayashi, K. Mizuno, H. Ohuchi, Appl. Catal. B: Environ. 12 (1997) 263–276.
[30] Y. Xu, B. Lei, L. Guo, W. Zhou, Y. Liu, J. Hazard. Mater. 160 (2008) 78–82.
[31] L. Jia, K. Fang, J. Chen, Y. Sun, React. Kinet. Catal. Lett. 93 (2008) 351–358.
[32] B. Erdem, R.A. Hunsicker, G.W. Simmons, E.D. Sudol, V.L. Dimonie, M.S. El-Aasser, Langmuir 17 (2001) 2664–2669.
[33] M. Watanabe, Y. Aizawa, T. Iida, R. Nishimura, H. Inomata, Appl. Catal. A: Gen. 295 (2005) 150–156.
[34] M.E. Manríquez, T. López, R. Gómez, J. Navarrete, J. Mol. Catal. A: Chem. 220 (2004) 229–237.
[35] M. Klimczak, P. Kern, T. Heinzelmann, M. Lucas, P. Claus, Appl. Catal. B: Environ. 95 (2010) 39–45.
[36] K. Nishiwaki, N. Kakuta, A. Ueno, H. Nakabayashi, J. Catal. 118 (1989) 498–501.
[37] M.C.J. Bradford, M.A. Vannice, Catal. Rev. Sci. Eng. 41 (1999) 1–42.
[38] T. Osaki, T. Moria, React. Kinet. Catal. Lett. 87 (2006) 149–156.

[39] A.H. de Morais Batista, F.F. de Sousa, S.B. Honorato, A.P. Ayala, J.M. Filho, F.W. de Sousa, A.N. Pinheiro, J.C.S. de Araujo, R.F. Nascimento, A. Valentini, A.C. Oliveira, J. Mol. Catal. A: Chem. 315 (2010) 86–98.
[40] H.-J. Freund, M.W. Roberts, Surf. Sci. Rep. 25 (1996) 225–273.
[41] G.C. Chinchen, M.S. Spencer, K.C. Waugh, D.A. Whan, J. Chem. Soc., Faraday Trans. 1 83 (1987) 2193–2212.
[42] C. Zhang, S. Li, L. Wang, T. Wu, S. Peng, Mater. Chem. Phys. 62 (2000) 52–61.
[43] K. Pokrovski, K.T. Jung, A.T. Bell, Langmuir 17 (2001) 4297–4303.
[44] A.E. Lisovskii, C. Aharoni, Catal. Rev. Sci. Eng. 36 (1994) 25–74.
[45] Y. Hirashima, K. Nishiwaki, A. Miyakoshi, H. Tsuiki, A. Ueno, H. Nakabayashi, Bull. Chem. Soc. Jpn. 61 (1988) 1945–1951.